Machine learning applied to wind turbine blades impact detection

Wind Engineering
XX(X):2–20

DOI: 10.1177/ToBeAssigned
www.sagepub.com/
SAGE

Congcong Hu[1] and Roberto Albertani[1]

Abstract

The significant development of wind power generation worldwide brings, together with environmental benefits, wildlife concerns for volant species vulnerability to interactions with wind energy facilities. For surveying such events, an automatic system for continuous monitoring of blade collisions is critical. An onboard multi-senor system capable of providing real-time collision detection using integrated vibration sensors is developed and successfully tested. However, to detect low signal-to-noise ratio impact can be challenging hence an advanced impact detection method has been developed and presented in this paper. A robust automated detection algorithm based on support vector machine is proposed. After a preliminary signal pre-processing, geometric features specifically selected for their sensitivity to impact signals are extracted from raw vibration signal and energy distribution graph. The predictive model is formulated by training conventional support vector machine using extracted features for impact identification. Finally, the performance of the predictive model is evaluated by accuracy, precision and recall. Results indicate a linear regression relationship between signal-to-noise ratio and model overall performance. The proposed method is much reliable on higher signal-to-noise ratio (SNR ≥ 6), but it shows to be ineffective at lower signal-to-noise ratio (SNR < 2).

Keywords

Wind turbine, birds, environment, vibration sensors, impact monitoring, machine learning, support vector machine

Prepared using sagej.cls *[Version: 2017/01/17 v1.20]*

Introduction

As an important component of renewable energy, wind energy generation has been growing at a fast pace in recent years due to its low cost and high availability (Kumar et al. 2016; Thaxter et al. 2017; Schwartz et al. 2010). **Although the environmental impact associated with the usage of fossil fuel can be reduced by the clean alternative energy source, the deployment of an increased number of wind facilities with larger scale turbines generates wildlife concerns for volant species such as birds and bats (Bailey et al. 2014; Thomsen 2014). Common causes of death for wildlife interacting with wind turbines include direct collision with turbines (Korner-Nievergelt et al. 2013; Parisé and Walker 2017; Zohbi et al. 2015; Smallwood 2017) and the risk of barotrauma especially for bats (Grodsky et al. 2011). Among all the causes, direct collision with wind turbines is the most visible and well-documented impact as results of wind energy development (Loss et al. 2013).**

Common methodologies applied at land-based wind farms for bird/bat fatality assessments are carcass surveys and long-term visual observation (e.g. Korner-Nievergelt et al. 2013; Parisé and Walker 2017; Smallwood 2017; Kunz et al. 2007), made generally at the scale of a single wind farm. Studies of bird and bat mortality rates from collisions with utility-scale wind turbines (e.g. K.Sovacool 2009; Marques et al. 2014) have reported an estimate of up to 40 deaths per turbine per year on certain sites. However, due to surveyor efficacy and carcass removal by scavengers, the count could be inaccurate, and the true magnitude of the problem could be underestimated (Smallwood 2017). Moreover, carcass survey and visual observation are characterized by high human operator's labor time, and are infeasible at certain sites, such as agricultural fields, dense shrub habitats, remote locations, and on water. Other methodologies (e.g. Sovacool et al. 2008; Plonczkier and Simms 2012; Brabant et al. 2015; Fijn et al. 2015; Towsey et al. 2014; Masden and Cook 2016) applied for estimation of potential interactions between volant species and wind facilities include aerial and boat-based visual surveys, radar monitoring, and acoustic recordings, which can be applied to collision risk models based on flux data. However, they are not suited for deterministic monitoring of collision events. Hence, effective and low-cost methods of continuous collision event monitoring with implementation of automatic data collection and evaluation have been sought by researchers in recent years (Marquez et al. 2012).

[1]School of Mechanical, Industrial and Manufacturing Engineering, Oregon State University, Corvallis, OR, USA

Corresponding author:
Roberto Albertani, School of Mechanical, Industrial and Manufacturing Engineering, Oregon State University, Corvallis, OR 97331, USA
Email: roberto.albertani@oregonstate.edu

Prepared using sagej.cls

Vibration-based monitoring techniques are widely adopted by modern wind turbines for rotating parts (e.g., brakes, bearings and gearboxes) (Marquez et al. 2012). Vibration sensors such as piezoelectric accelerometers are commonly installed on wind turbines for the analysis of dynamic structural response during operations (Bassett et al. 2011; Abouhnik and Albarbar 2012). One notable approach for volant species collision detection is the conceptual design of a multi-sensor system developed by the authors (Hu et al. 2018). By implementation of vibration sensors and surveillance cameras, the multi-sensor system can perform on-board collision detection, providing information for taxonomic identification, with minimal effort required to maintain long operational life. The preliminary results of field testing on utility-scale wind turbines proved the feasibility of collision detection using vibration sensors (Hu et al. 2018). However, advanced signal processing methods need to be developed for a higher detection rate, especially for those impacts with relatively low signal-to-noise ratio (SNR), which typically involve bats and small birds such as the Marbled Murrelet.

Support vector machine (SVM) is one of the most widely applied frameworks for general classification problems such as condition monitoring and fault diagnosis (Cristianini 2000). Relevant features of an event can be extracted and then represented as a vector in SVM feature space. Non-probabilistic binary linear classifiers allow SVM to divide the feature space into different categories, enabling automatic prediction of a future event on its member category.

This paper presents a robust signal processing method based on SVM applied to automated impact detection. Firstly, geometric features associated with structure characteristics of impact signals are extracted from both raw vibration signals and energy distribution graph. Input vectors constructed by extracted features are then applied to train the SVM model, which is used for impact identification after training. The objectives of this study are to illustrate signal qualities of common vibration sensors on non-stationary wind turbine blades, and to evaluate the feasibility of proposed automated impact detection method using conventional support vector machine, especially for different levels of SNR.

The remainder of this paper is organized as follows. The theoretical background and proposed procedure are briefly described in section 2. Section 3 introduces the experimental data acquisition system, discusses field testing results, and illustrates the pre-processing methods on field-collected raw signals. To overcome the issue of rarity of bird collision events and limited number of artificial impacts, simulated studies are performed in Section 4. Finally, conclusions are drawn in Section 5.

Theoretical Background

Support Vector Machine

SVM is a supervised machine learning method introduced by Boser, Guyon and Vapnik (1992), which is widely used in machine condition monitoring and fault diagnosis. The process of SVM for a binary

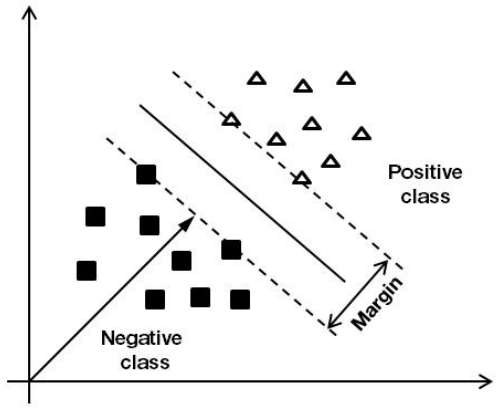

Figure 1. Illustration of linear classifier in two-dimensional space.

classification problem is described as follows. Assume a sample dataset $(x_i, y_i)_{i=1}^{N}$, where the notation x_i denotes the i^{th} vector in the dataset and y_i is the label associated with x_i. In binary classification, the positive and negative classes are labeled with $y_i = 1$ and $y_i = -1$, respectively. The discriminant function is of the form

$$f(x) = w^T x + b, \tag{1}$$

where w is the weight vector, and b is the bias. Based on the discriminant function, a hyperplane defined by

$$f(x) = w^T x + b = 0 \tag{2}$$

divides the input space X into two classes: positive ($f(x) > 0$) and negative ($f(x) < 0$). To find the optimal hyperplane, the maximum margin criterion is applied, by which the optimal hyperplane is the hyperplane that gives the maximum distance between the decision boundary and the plane, as illustrated in Figure 1.

Considering noisy data that are not linearly separable, or to achieve a larger margin, misclassification is allowed by introducing slack variables $\xi_i > 0$ and error penalty $C > 0$. The problem can be expressed by the following constrained optimization problem:

$$\begin{aligned} &\text{Minimize} && \frac{1}{2}\|w\|^2 + C\sum_{i=1}^{n}\xi_i \\ &\text{subject to} && y_i(w^T x_i + b) \geq 1 - \xi_i \end{aligned} \tag{3}$$

which is also known as soft-margin SVM (Cristianini 2000). Introducing Lagrange multipliers α_i, this optimization problem can be converted into the equivalent Lagrange dual formulation:

$$\begin{aligned} &\text{Minimize} && L(\alpha) = \sum_{i=1}^{N}\alpha_i - \frac{1}{2}\sum_{i=1}^{N}\alpha_i\alpha_j y_i y_j x_i^T x_j \\ &\text{subject to} && \sum_{i=1}^{N}\alpha_i y_i = 0,\ 0 \leq \alpha_i \leq C. \end{aligned} \tag{4}$$

To define a nonlinear classifier, the input vector x_i is mapped from lower input space X into higher feature space F by mapping function $\Phi(x)$, which typically calculates using a dot product. However, the approach of explicitly mapping each input vector from the input space into the feature space results in quadratic complexity (i.e., quadratic increase in memory usage and quadratic increase in time required for computation). The kernel function $K(x_i, x_j) = \Phi^T(x_i) \cdot \Phi(x_j)$ is then introduced to solve the issue by skipping the step of explicitly mapping. The following four basic kernels are most commonly used:

- linear: $K(x_i, x_j) = x_i^T x_j$,
- polynomial: $K(x_i, x_j) = (\gamma x_i^T x_j + r)^d, \gamma > 0$,
- radial basis function (RBF): $K(x_i, x_j) = exp(-\gamma\|x_i - x_j\|^2), \gamma > 0$,
- sigmoid: $K(x_i, x_j) = tanh(\gamma x_i^T x_j + r)$.

The RBF kernel is generally preferred (Cristianini 2000) and is applied in the present work.

Finally, the problem is converted into a "kernelized" dual quadratic optimization problem as follows:

$$\begin{aligned} &\text{Minimize} && L(\alpha) = \sum_{i=1}^{N}\alpha_i - \frac{1}{2}\sum_{i=1}^{N}\alpha_i\alpha_j y_i y_j K(x_i, x_j) \\ &\text{subject to} && \sum_{i=1}^{N}\alpha_i y_i = 0,\ 0 \leq \alpha_i \leq C. \end{aligned} \tag{5}$$

This problem can be solved by the method of sequential minimal optimization (Cristianini 2000). The final discriminant function then has the expression of

$$f(x) = sign(\sum_{i=1}^{N} \alpha_i y_i K(x, x_i) + b). \tag{6}$$

Procedure for Impact Detection

In the present study, SVM has been proposed as the classification method; the procedure for the automatic impact detection using SVM is shown in Figure 2. The following steps are applied: 1) Raw vibration signal is collected by vibration sensors installed on the wind turbine blades; 2) Raw signal is pre-processed using continuous wavelet transform (CWT); 3) The time marginal integration (TMI) graph is obtained by calculating the energy distribution in CWT with respect to time (i.e., integrating CWT with respect to time for each scale); 4) Features are extracted from both raw signal and TMI graphs. The selected 18 features (Kumar and Kumar 2017) are listed in Table 1; 6) The SVM model is trained and tested by 10-fold cross-validation. Parameters γ and C are optimized by grid search in a grid of $2^{-10} - 2^{10}$.

Experimental Evaluation

System Setup and Data Acquisition

The conceptual design of the on-board multi-sensor system under daylight operations was developed by the authors (Hu et al. 2018). It primarily consists of: 1) Vibration sensor node (accelerometers) installed on the root of the blade, 2) Optical node (surveillance cameras) aiming at the rotor plane, 3) Bioacoustics node (acoustic microphones) mounted outside the nacelle, and 4) Data acquisition system and central controller inside the nacelle. The vibration sensors provide continuous vibration monitoring, while the optical and acoustic nodes acquire necessary information (i.e., visual images, impact sounds, and animal calls) for event confirmation and species recognition when an impact is detected. The event-driven trigger architecture was used to acquire data since continuous data acquisition by the optical node at frame rates sufficient to capture fast-moving objects will produce a prohibitory volume of data to be archived. Each node continuously streams data into a ring buffer for temporary storage. When an event (e.g., collision/impact) is registered by the vibration node, all buffers will store data in an operator-determined time window, which eventually will be asynchronously stored on disk. This architecture minimizes the volume of data archived and enhances efficiency of data post-processing.

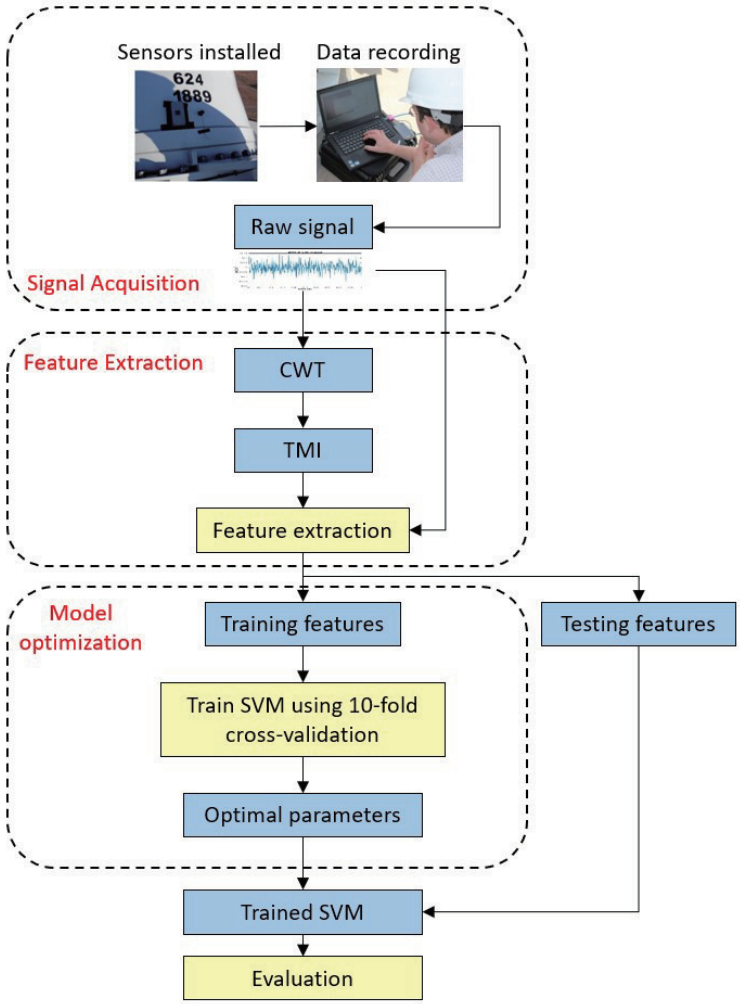

Figure 2. Flow chart of procedure for impact detection.

Blade vibrations were selected as the primary triggering source of the system. Wireless three-axis accelerometers (LORD MicroStrain G-Link LXRS w/ 104-LXRS base station) were installed at the root of each blade with weatherproof housing, as shown in Figure 3. The installation position was selected for easier accessible installation and maintenance, and negligible aerodynamic effects on the blades. For timely processing of data for real-time collision monitoring, considering the processing capabilities of the selected hardware, sampling rates were chosen at 512 Hz (Bassett et al. 2011).

Table 1. List of extracted features.

No.	Feature	Source
1	Kurtosis	Raw signal
2	Skewness	
3	Mean	
4	RMS	
5	Variance	
6	Peak	
7	Impulse factor	
8	Shape factor	
9	Crest factor	
10	Kurtosis	TMI signal
11	Skewness	
12	Mean	
13	RMS	
14	Variance	
15	Peak	
16	Impulse factor	
17	Shape factor	
18	Crest factor	

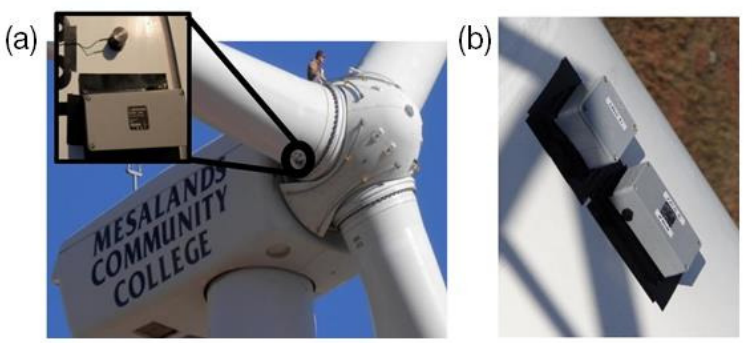

Figure 3. Experimental set-up of data acquisition system: (a) Installation of vibration node at the root of each blade; (b) housing of vibration node.

The overall system functionality, reliability, and accuracy were validated in field tests with operating wind turbines and simulated bird impacts on the blades. Two sites for field testing were selected for availability of wind turbines not involved in commercial energy conversion and for the excellent technical and logistic support on site. Partial system early tests were performed at the North American Wind

Figure 4. Simulation of bird impacts by launching tennis balls using an air cannon.

Research and Training Center (NAWRTC) at the Mesalands Community College in Tucumcari, NM, on a General Electric (GE) 1.5 MW wind turbine. Later tests on the fully integrated system were performed at the National Renewable Energy Laboratory (NREL) National Wind Technology Center (NWTC) in Boulder, CO. The turbine used at the NWTC was the 600 kW CART3 (three blades). In both cases, bird impacts were simulated by launching tennis balls using a custom compressed-air cannon, as illustrated in Figure 4. The cannon was barreled to the size of a regular tennis ball, whose mass was 57 g and 140 g when filled with water.

Development costs of the general system were covered by funds from the U.S. Department of Energy. Material costs, without considering improvement due to manufacturing efficiency and mass production, are estimated to be approximately 700 to 1,000 U.S. dollars per blade plus the cost for a computer laptop per turbine, after fixed costs for production tools are covered. Installation on a large size wind turbine requires approximately two persons for two to three days, including system set up and basic functional tests. Real time blade-events monitoring is automatic including uploading of data and images to a storage system, cloud-based or similar, providing network or satellite link is available. Post events inspection of recorded images is currently based on visual interaction with human operators after the images are available after recording. Automatic computer-based inspection is possible as future development. Additionally, since blade damage was the most frequently reported damage occurrences among all other subsystems (i.e., gearbox, generator, transformer, foundation and other) (Shohag et al. 2017), the proposed system may also serve for blade health monitoring. However, it will require better understanding on the turbine and

Table 2. Overview of SNR for all impacts.

Case	# of impacts	Avg. SNR (dB)	CV (%)
CART3 600 kW normal operation	6	5.45	35.74
CART3 600 kW idle operation	4	14.59	37.01
GE 1.5 MW normal operation	23	7.03	33.05

blade structures (Sellami et al. 2016) and further development of implemented diagnosis algorithms (Ouanas et al. 2018; Purarjomandlangrudi et al. 2013).

Summary of Field Testing Results

Due to varying wind conditions, low impact rate, and short timeframe of field testing, a limited number of collision events was created and recorded. All recordings were manually triggered to ensure that the raw signal was collected for later examination and post-processing. Field notes of visually observed impact events including time, position of impact, blade status, and weather conditions were recorded and matched with output signals acquired from each sensor node. Preliminary examination, including visual inspection and signal processing using the short-time Fourier transform (STFT), was performed on-site on raw signals. In summary, 23 dynamic impact events (i.e., moving blade hitting tennis balls) were successfully obtained at NAWRTC, and six were obtained at NWTC under wind turbine normal operating condition (i.e., rotor at designed speed, generator engaged). The higher impact rate at NAWRTC was primarily caused by more favorable wind conditions. Likewise, four additional dynamic impact events were recorded at NWTC under turbine idle operation (i.e., rotor free spinning, generator not engaged) due to low wind occurrence.

Raw signal examples of a blade striking a tennis ball are shown in Figure 5. The three time histories represented from top to bottom are (a) NREL CART3 during normal operations producing energy, (b) NREL CART3 during idle with generator disengaged, and (c) NAWRTC GE during normal operations producing energy. Table 2 lists the results of average SNR and the corresponding coefficient of variation (CV) for each testing case. The SNR was defined as follows:

$$\text{SNR} = 20log_{10}\frac{A_{\text{impact}}}{A_{\text{noise}}} \tag{7}$$

where A is the root mean square (RMS) amplitude and was calculated and evaluated for signal with impacts. In all three plots in Figure 5, the spikes of impact were slightly ahead of the triggering events due to the reaction time of the recorder. As expected, signals collected under idle operations are characterized

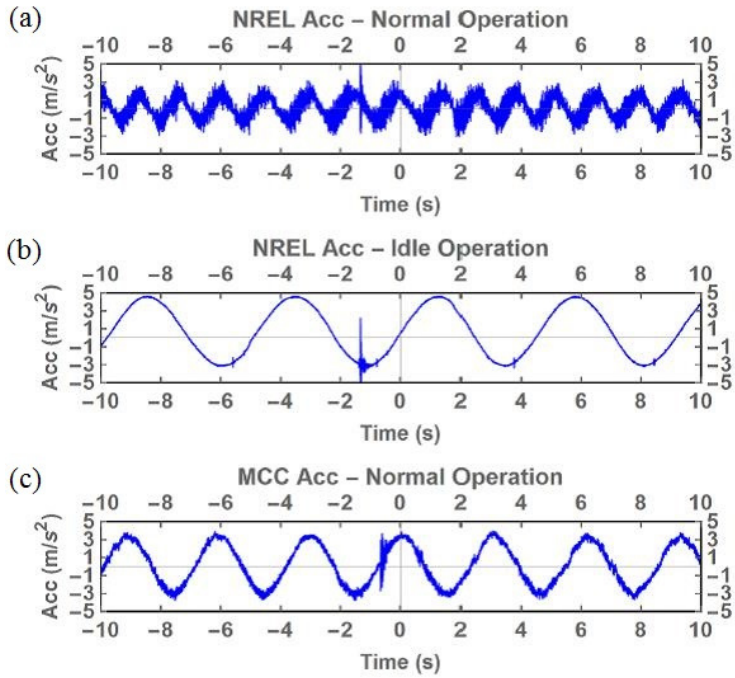

Figure 5. Illustration of vibration signals from accelerometers with different background noise: (a) NREL CART3 during normal operations producing energy; (b) NREL CART3 during idle operation with blade free spinning; (c) NAWRTC GE during normal operations producing energy.

with a lowest background vibration noise, resulting in a highest SNR due to the disengagement of the generator and low-power operation of the gearbox.

Over the 29 blade-strike events under normal operation, only 14 can be confirmed by visual inspection, as illustrated in Figure 5, and by STFT. The most probable cause of this partial detection rate was the low-energy characteristic of several events due to the location of the impact close to the rotor shaft, which results in a significantly low SNR that cannot be identified using preliminary examination techniques. Most of the detected strikes occurred at the leading edge of the blade and in a radial position between half blade and blade tip, thus at relatively high kinetic energy. Impacts during turbine idle operations are particularly favorable for detection due to the extremely low background noise measured by the sensors.

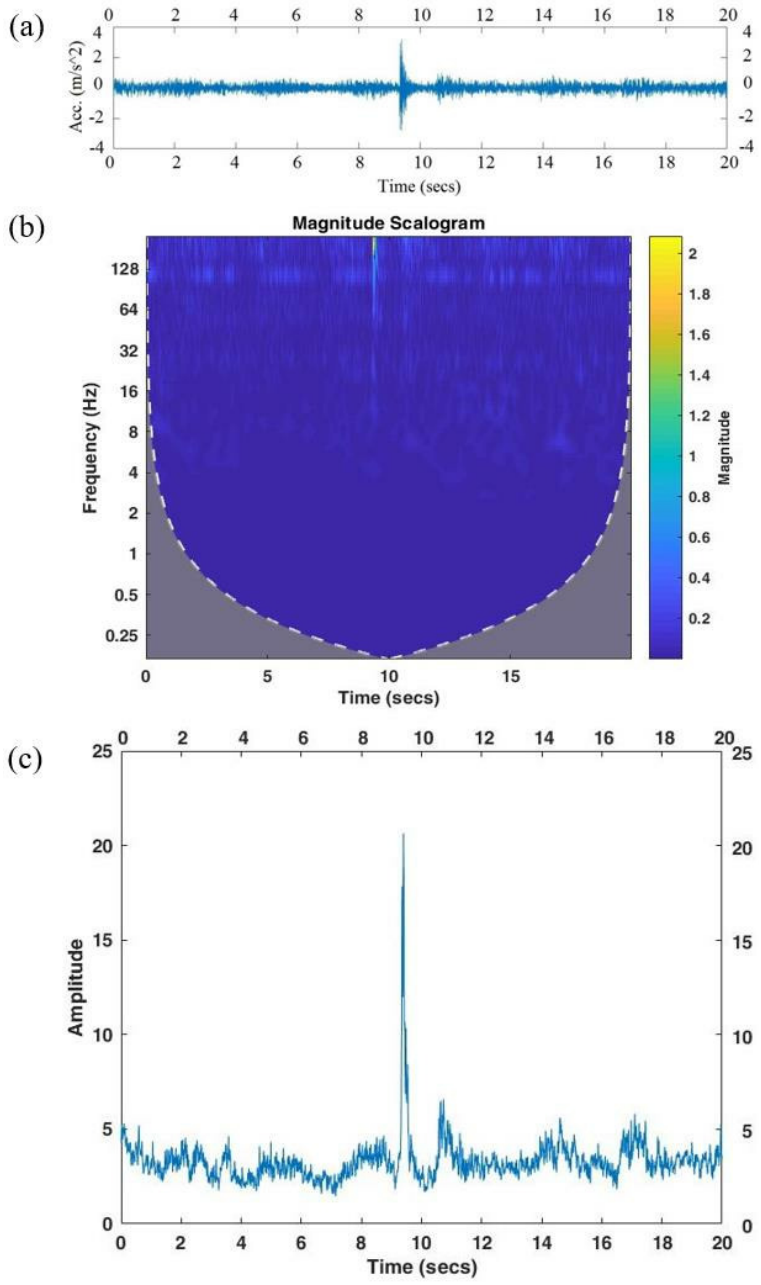

Figure 6. Combination of three graphs showing a) Time-series plot, b) Wavelet plot and c) Integration of wavelet respect to frequency, respectively, for NAWRTC GE turbine during normal operation.

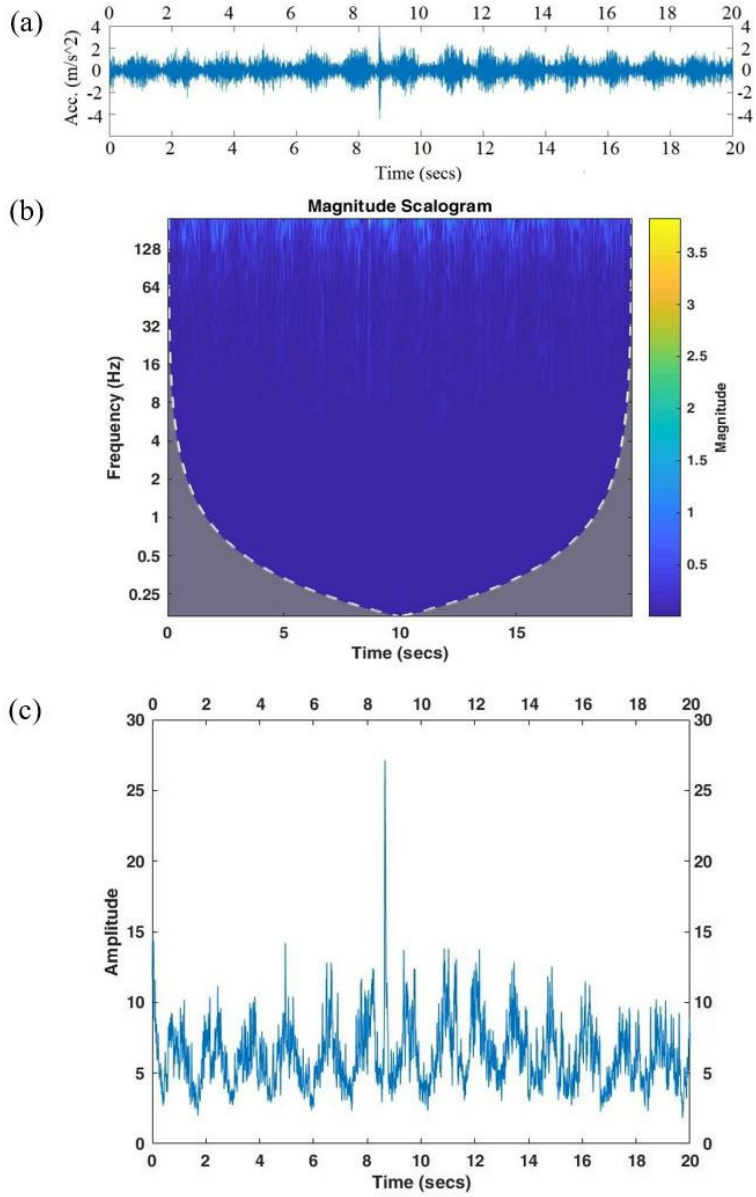

Figure 7. Combination of three graphs showing a) Time-series plot, b) Wavelet plot and c) Integration of wavelet respect to frequency, respectively, for NREL CART3 during normal operation.

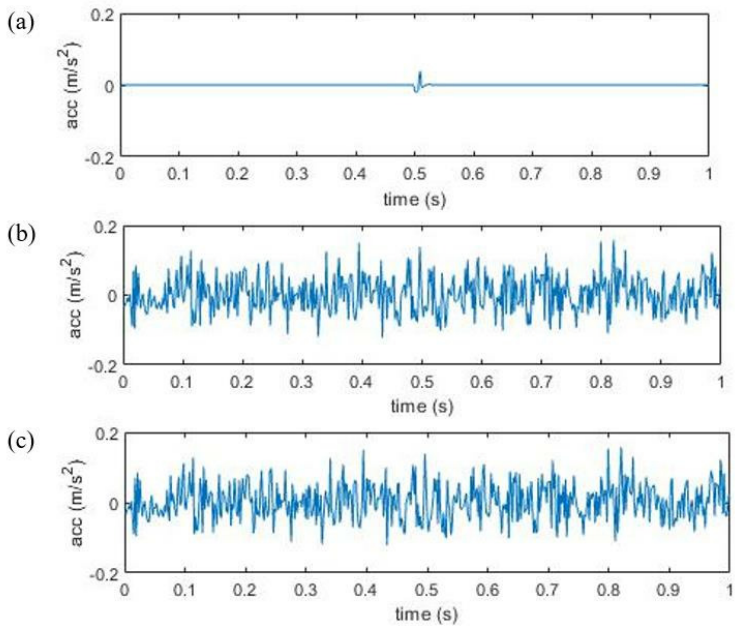

Figure 8. The waveform of constructed signal with SNR=1.5: (a) single impact with ξ=0.007 and f=512 Hz; (b) Gaussian white background noise with zero-mean and 0.05 standard deviation; (c) mixed signal.

Pre-processing of Raw Signals

For SVM data preparation, the raw signals were pre-processed. Figure 6 and Figure 7 illustrate the pre-processing steps using raw signals from both the GE and CART3 turbines under normal operation. The raw time histories of Figure 6 and Figure 7 are shown in Figure 5 bottom and top, respectively. A high-pass filter was applied to eliminate low-frequency components ($f \leq 5$ Hz) caused by blade rotation. Resultant time histories are shown in Figure 6(a) and Figure 7(a). This step was applied to eliminate the considerably large kinetic energy caused by blade rotation, which can easily dominate the energy distribution graph if presented. Figure 6(b) and Figure 7(b) show the scalograms as results of the continuous wavelet transform (CWT). CWT gives overall better time resolution for high-frequency components, which is essential for obtaining the energy distribution graph when integrating CWT with respect to time. Figure 6(c) and Figure 7(c) are the energy distribution plots illustrated by TMI graphs. It is noted that impacts are better distinguishable in TMI graphs than in CWT plots. Features listed in Table 1 are then extracted from the raw signal and the TMI graph to obtain a training and testing dataset.

Simulated Studies

Since bird/bat impacts are rare, artificial impacts were created by launching tennis balls using a compressed-air cannon. Ideally, the vibration sensors need to be installed on turbine blades for a sufficient time to obtain both signals with and without artificial impacts. However, even with artificial impacts, only a handful of events were successfully created, as stated in the previous section. The predictive model developed by such imbalanced dataset can be biased and inaccurate (Cristianini 2000), especially when the detection of the impact is crucial. Hence, mathematically simulated impact events were conducted for a sufficient number of training examples from both positive (i.e., impact events) and negative (i.e., non-impact events) categories. In the simulation, a single impact signal is defined as:

$$s(t) = \begin{cases} 0 & t < 0 \\ exp(-\frac{\xi}{\sqrt{1-2\xi^2}} \cdot 2\pi f t) \cdot sin(2\pi f t) & t \geq 0 \end{cases}, \tag{8}$$

where ξ is the damping coefficient, $\frac{\xi}{\sqrt{1-2\xi^2}}$ is the damping attenuation characteristics of impact response, and f is the sampling frequency (Liu et al. 2016). The background noise is simulated using Gaussian white noise, which can be characterized by its mean and standard deviation. Figure 8 shows the waveform of the simulation signal with $\xi = 0.007$ and $f = 512$ Hz for the single impact signal, Gaussian white background noise with zero-mean and 0.05 standard deviation, and the mixed signal, respectively. A total number of 10,000 independent examples (5,000 with impact and 5,000 without impact) were simulated for each level of SNR. The SVM model was built using 10-fold cross-validation and evaluated by traditional evaluation methods including:

$$Accuracy = \frac{TP + TN}{TP + TN + FP + FN}, \tag{9}$$

$$Precision = \frac{TP}{TP + FP}, \tag{10}$$

$$Recall = \frac{TP}{TP + FN}, \tag{11}$$

where TP, TN, FP, FN are true positive, true negative, false positive, and false negative events, respectively. Figure 9 and Figure 10 show the relationships between SNR and $accuracy$, SNR and $precision$, respectively. In both plots, the first three datapoints (SNR < 2) are considered as outliers since an approximate of 50% or less detection rate in a binary classification case indicates nothing more than a random guess. In other words, the predictive model is underfitting when the impact signal is too small. For SNR ≥ 2, both plots exhibit linear regression relationships between SNR and $accuracy$, SNR

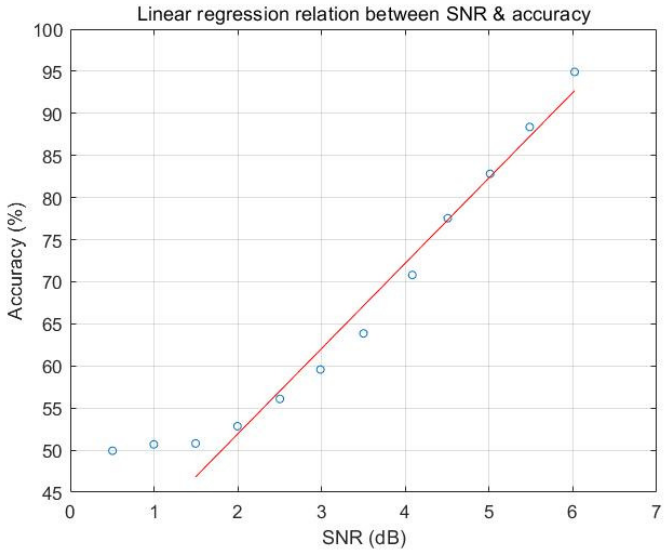

Figure 9. Relationship between SNR and accuracy. Each point represents the resultant of 10,000 independent examples.

and $precision$, respectively. As expected, the overall performance of the predictive model increases as the SNR increases.

It should be noted that in the case of avian species interacting with wind turbines, the detection of impact is crucial for the purpose of bird protection since data and images for event confirmation and species recognition will only be available when the system is triggered (Hu et al. 2018). That means the detection system will prefer to detect all actual impacts (i.e., TP plus FN) but can allow some tolerance in the accuracy of non-impact event detection. Hence, $recall$ is of greater importance when evaluating the model performance. Figure 11 shows the relationship between SNR and $recall$. The first three datapoints are still considered as outliers despite a detection rate slightly over 50%. For SNR ≥ 2, the plot also exhibits linear regression relationships between SNR and $recall$, which is in consistence with the results of performance evaluated by $accuracy$ and $precision$.

Conclusions

This study demonstrates through both experimentation and simulation the feasibility of impact detection using a conventional SVM model applied to vibration data collected by vibration sensors on wind turbine blades. Field tests were performed on full-scale wind turbines in real operating conditions with simulated

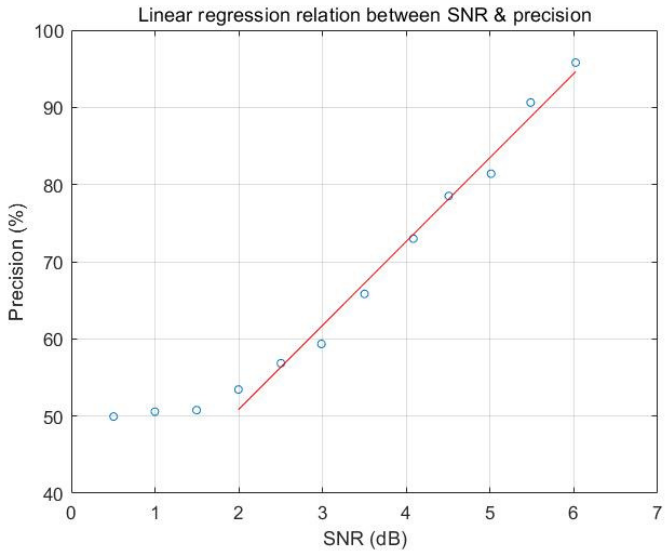

Figure 10. Relationship between SNR and precision. Each point represents the resultant of 10,000 independent examples.

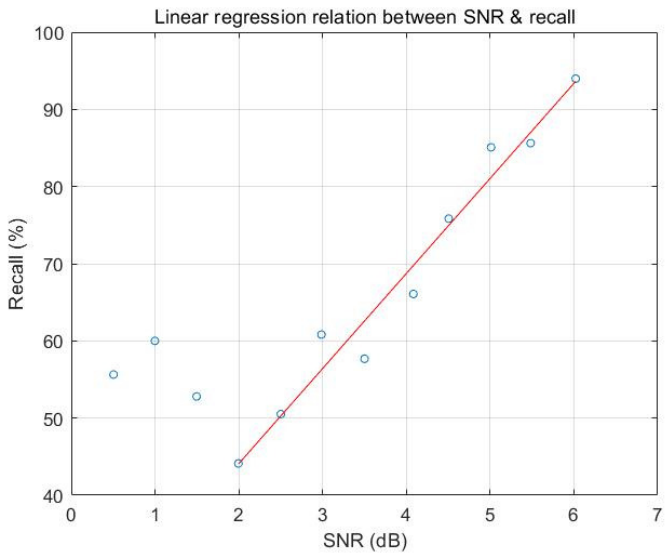

Figure 11. Relationship between SNR and recall. Each point represents the resultant of 10,000 independent examples.

bird impact on blades. 14 out of 29 registered artificial impacts were identified on-site by visual inspection and signal processing using the short-time Fourier transform on raw vibration signal time histories, which corresponds to a 48.3% success rate. It elucidates that SNR, together with a fast post-processing technique to discern the spike caused by the impact from the normal vibration background, are critical for real-time automatic impact detection on wind turbine blades. It is necessary to perform simulated studies due to the fact that bird impacts are rare. Simulated studies also allow the performance evaluation of SVM model on lower SNRs, which is not feasible using field testing data since the impact signals are usually indistinguishable. It can be concluded from simulated studies that the proposed SVM model trained by the 18 features extracted from raw vibration time histories and TMI graph can reliably predict whether a sample signal contains an impact or not, with an overall $accuracy$, $precision$ and $recall$ higher than 95% when SNR ≥ 6. However, the model is not effective when SNR < 2.

Acknowledgements

The authors wish to acknowledge the financial support of the U.S. Department of Energy under DE-EE0005363. The authors are grateful to the staff of the North American Wind Research and Training Center at Mesalands Community College for contributing to the success of the system's first field test. The authors would also like to express gratitude to the staff and scientists at NREL for their willingness to share information with the team and for use of the Controls Advanced Research Turbines (CART) at the National Wind Technology Center for system testing and demonstration. Finally, we greatly appreciate the review and expert contributions of our science and industry advisory panel.

References

Abouhnik A and Albarbar A (2012) Wind turbine blades condition assessment based on vibration measurements and the level of an empirically decomposed feature. *Energy Conversion and Management* 64: 606–613.

Bailey H, Brookes KL and Thompson PM (2014) Assessing environmental impacts of offshore wind farms: lessons learned and recommendations for the future. *Aquatic Biosystems* 10(1): 8.

Bassett K, Carriveau R and Ting DS (2011) Vibration response of a 2.3 mw wind turbine to yaw motion and shut down events. *Wind Energy* 14(8): 939–952.

Boser BE, Guyon IM and Vapnik VN (1992) A training algorithm for optimal margin classifiers. In: Haussler D (ed.) *Proceedings of the 5th Annual Workshop on Computational Learning Theory (COLT'92)*. Pittsburgh, PA, USA: ACM Press, pp. 144–152.

Brabant R, Vanermen N, Stienen EWM and Degraer S (2015) Towards a cumulative collision risk assessment of local and migrating birds in north sea offshore wind farms. *Biological Conservation* 756(1): 63–74.

Cristianini N (2000) *An introduction to support vector machines : and other kernel-based learning methods*. Cambridge, New York: Cambridge University Press.

Fijn RC, Krijgsveld KL, Poot MJM and Dirksen S (2015) Bird movements at rotor heights measured continuously with vertical radar at a dutch offshore wind farm. *IBIS* 157(3): 558–566.

Grodsky SM, Behr MJ, Gendler A, Drake D, DDieterle B, Rudd RJ, Walrath NL and Jacobs DS (2011) Estimates of bird collision mortality at wind facilities in the contiguous united states. *Journal of Mammalogy* 92(5): 917–925.

Hu C, Albertani R and Suryan RM (2018) Wind turbine sensor array for monitoring avian and bat collisions. *Wind Energy* 21: 255–263.

Korner-Nievergelt F, Brinkmann R, Niermann I and Behr O (2013) Estimating bat and bird mortality occurring at wind energy turbines from covariates and carcass searches using mixture models. *PLOS ONE* 8(7).

KSovacool B (2009) Contextualizing avian mortality: A preliminary appraisal of bird and bat fatalities from wind, fossil-fuel, and nuclear electricity. *Energy Policy* 37(6): 2241–2248.

Kumar A and Kumar R (2017) Time-frequency analysis and support vector machine in automatic detection of defect from vibration signal of centrifugal pump. *Measurement* 108: 119–133.

Kumar Y, Ringenberg J, Depuru SS, Devabhaktuni VK, Lee JW, Nikolaidis E, Andersen B and Afjeh A (2016) Wind energy: Trends and enabling technologies. *Renewable and Sustainable Energy Reviews* 53: 209–224.

Kunz T, Arnett EB, Cooper BM, Erickson WP, Larkin RP, Mabee T, Morrison ML, Strickland MD and Szewczak JM (2007) Assessing impacts of wind-energy development on nocturnally active birds and bats: A guidance document. *Journal of Wildlife Management* 71(8): 2449–2486.

Liu R, Yang B, Zhang X, Wang S and Chen X (2016) Time-frequency atoms-driven support vector machine method for bearings incipient fault diagnosis. *Mechanical System and Signal Processing* 75: 345–370.

Loss SR, Will T and Marra PP (2013) Estimates of bird collision mortality at wind facilities in the contiguous united states. *Biological Conservation* 168: 201–209.

Marques AT, Batalha H, Rodrigues S, Costa H, Pereira MJR, Fonseca C, Mascarenhas M and Bernardino J (2014) Understanding bird collisions at wind farms: An updated review on the causes and possible mitigation strategies. *Biological Conservation* 179: 40–52.

Marquez FPG, Tobias AM, Perez JMP and Papaelias M (2012) Condition monitoring of wind turbines: Techniques and methods. *Renewable Energy* 46: 169–178.

Masden EA and Cook ASCP (2016) Avian collision risk models for wind energy impact assessments. *Environmental Impact Assessment Review* 56: 43–49.

Ouanas A, Medoued A, Mordjaoui M, Lebaroud A and Sayad D (2018) Fault diagnosis in yaw drive induction motor for wind turbine. *Wind Engineering* 42(6): 576–595.

Parisé J and Walker TR (2017) Industrial wind turbine post-construction bird and bat monitoring: A policy framework for canada. *Journal of Environmental Management* 201: 252–259.

Plonczkier P and Simms IC (2012) Radar monitoring of migrating pinkfooted geese: behavioural responses to offshore wind farm development. *Journal of Applied Ecology* 49(5): 1187–1194.

Purarjomandlangrudi A, Nourbakhsh G, Esmalifalak M and Tan A (2013) Fault detection in wind turbine: A systematic literature review. *Wind Engineering* 37(5): 535–546.

Schwartz M, Heimiller D, Haymes S and Musial W (2010) Assessment of offshore wind energy resources for the united states. Technical report, National Renewable Energy Laboratory, Golden, CO.

Sellami T, Berriri H, Darcherif AM, Jelassi S and Mimouni MF (2016) Modal and harmonic analysis of three-dimensional wind turbine models. *Wind Engineering* 40(6): 518–527.

Shohag MA, Hammel EC, Olawale DO and Okoli OI (2017) Damage mitigation techniques in wind turbine blades: A review. *Wind Engineering* 41(3): 185–210.

Smallwood KS (2017) Long search intervals underestimate bird and bat fatalities caused by wind turbines. *Wildlife Society Bulletin* 41(2): 224–230.

Sovacool BK, Lindboe HH and Odgaard O (2008) Is the danish wind energy model replicable for other countries? *The Electricity Journal* 21(2): 27–38.

Thaxter CB, Buchanan GM, Carr J, Butchart SHM, Newbold T, Green RE, Tobias JA, Foden WB, O'Brien S and Pearce-Higgins JW (2017) Bird and bat species' global vulnerability to collision mortality at wind farms revealed through a trait-based assessment. *Proc. R. Soc. B* 284(1862).

Thomsen K (2014) *Offshore wind : A comprehensive guide to successful offshore wind farm installation*. San Diego, CA: Elsevier Science.

Towsey M, Wimmer J, Williamson I and Roe P (2014) The use of acoustic indices to determine avian species richness in audio-recordings of the environment. *Ecological Informatics* 21: 110–119.

Zohbi GA, Hendrick P and Bouillard P (2015) Evaluation of the impact of wind farms on birds: The case study of lebanon. *Renewable Energy* 80: 682–689.